Zn, Ce, Pr, and Th doping in $YBa_2Cu_4O_8$

X. Zhang, K. W. Yip, and C. K. Ong
Department of Physics, National University of Singapore, Lower Kent Ridge Road, Singapore 0511, Republic of Singapore
(Received 27 June 1994; revised manuscript received 6 September 1994)

Computer-simulation techniques have been used to study Zn, Ce, Pr, and Th doping in $YBa_2Cu_4O_8$. Our results suggest that Zn energetically prefers to substitute at the Cu(2) site whereas Pr and Th prefer to substitute at the Y site. These results are in agreement with the experimental results. Our results also suggest that Ce preferentially substitutes for the Cu(2) site. The changes in interatomic distances caused by Zn, Ce, Th, and Pr doping were also presented and analyzed. Our calculated changes in lattice parameters of $YBa_2Cu_4O_8$ due to Th and Ce doping are in qualitative agreement with the experimental results.

INTRODUCTION

The crystal structure of the $YBa_2Cu_4O_8$ superconductor is similar to that of $YBa_2Cu_3O_{7-x}$ except for the presence of CuO double chains along its b axis. A unique character of this double-chain structure is a strong bond of the chain oxygen atoms [O(4) and O(4′)] with the Cu(1) atoms, resulting in a very good thermal stability with respect to the oxygen stoichiometry. This makes $YBa_2Cu_4O_8$ particularly stable against phase transitions involving changes in the oxygen sublattice as a function of temperature or pressure. $YBa_2Cu_4O_8$ is a very interesting high-T_c superconductor, as its T_c can be changed by pressure or by cation doping. The T_c for $YBa_2Cu_4O_8$ has been shown to increase on application of pressure with a very large dT_c/dP of 5.5 K GPa^{-1}.[1] The T_c passes through a maximum of $\sim$108 K at pressure of 9–10 GPa.[2–4] The T_c can be enhanced by Ca doping. It has been reported that Ca mainly doped at the Y site.[5,6] Some other studies show that Ca dopes at the Ba site.[7–9] The T_c for $YBa_2Cu_4O_8$ can also be depressed by Fe,[10–12] Co,[13] and Ni (Ref. 14) doping. The effect of Sr doping is different from the above cation dopants. Some research workers reported that the T_c of $YBa_2Cu_4O_8$ is nearly independent of Sr doping;[15,16] another work reported that T_c increased from 85 K ($x=0$) to 90 K ($x=0.1$–0.2) and then decreased to 64 K at $x=0.5$.[17]

Computer-simulation techniques have been used to study a range of cation dopants (Ca, Sr, Fe, Co, Ni, Mg, and Mn) in $YBa_2Cu_4O_8$.[18–20] It is found that the structural changes due to doping by Ca and Sr are very different from those caused by other cation dopants. The structural change caused by Ca is similar to those due to high pressure. The enhancement of T_c upon Ca doping may be attributed to the same mechanism as proposed for the enhancement of T_c under pressure.

Recently some more cation dopants have been found to depress T_c of $YBa_2Cu_4O_8$. Zn dopant is found to depress T_c with a coefficient of -21 K/at. % and it resides in the Cu(2) site.[21–23] Substitution of Ce at Y sites cause a decrease in T_c as well.[24] The deleterious influence of Th substitution at Y sites has also been reported.[25] The effect of Pr substitution was studied and it is reported that substitution of Pr at Y sites depresses T_c as well.[26–28] In this paper, we will use computer-simulation techniques to investigate the structural changes caused by Zn, Ce, Th, and Pr doping in $YBa_2Cu_4O_8$.

COMPUTATIONAL METHOD

Our simulation is based on the shell-model generalization of the Born model of the solid, which treats the solid as a collection of point ions with short-range repulsive forces acting between them. This approach has achieved a wide range of success, although, naturally, the reliability of the simulations depends on the validity of the potential model used in the calculations. Detailed discussion of this simulation technique can be found in Ref. 29. Many of the key ideas and applications are given in the papers honoring 50 years of the Mott-Littleton method.[30] We shall only give a brief description of the interatomic potentials and defect energy calculation.

The short-range potentials used in this classic simulation are described by the Born-Mayer potential supplemented by an attractive r^{-6} term:

$$V(r)=A\exp(-r/\rho)-Cr^{-6}, \tag{1}$$

where A, ρ, and C are constants. The polarizability of individual ions and its dependence on local atomic environment are treated by the shell model,[31] in which the outer valence cloud of the ion is simulated by a massless shell of charge Y and the nucleus and inner electrons by a core of charge X. The total charge of the ion is thus $X+Y$, which indicates the oxidation state of the ion. The interaction between core and shell of any ion is treated as harmonic with a spring constant k and represented by

$$V(r_i)=\tfrac{1}{2}k_i d_i^2, \tag{2}$$

where d_i is the relative displacement of core and shell of ion i. The electronic polarizability of the free ion i is thus given by

$$\alpha_i=Y_i^2/k_i, \tag{3}$$

where Y_i is the shell parameter. In this work, we treated the defective lattice by using the two-region strategy.[32] In this approach the crystal is formally divided into an

TABLE I. Potential parameters for $YBa_2Cu_4O_8$. All short-range potentials are set to zero for $r > 5.76$ Å. XX^- are the labels for O(1), O(4), and O(4'). Note the free-ion polarizability $\alpha = Y^2/K$.

	Short-range interaction		
	A (eV)	ρ (Å)	C (eV Å^6)
O^{2-}-O^{2-}	22 764.0	0.149 0	25.0
O^{2-}-XX^-	22 764.0	0.149 0	25.0
XX^--XX^-	22 764.0	0.149 0	25.0
O^{2-}-Cu^{2+}	2 068.04	0.268 76	0.0
O^{2-}-Ba^{2+}	2 104.1	0.354 77	0.0
O^{2-}-Y^{3+}	19 542.27	0.244 15	0.0
XX^--Cu^{2+}	2 486.04	0.257 53	0.0
XX^--Ba^{2+}	93 869.0	0.221 35	0.0
Cu^{2+}-Ba^{2+}	168 128.6	0.228 73	0.0
Ba^{2+}-Ba^{2+}	2 663.7	0.255 8	0.0

	Shell-model parameters	
Species	Y (e)	k (eV Å^{-2})
Cu^{2+}	2.0	999 999.0
Y^{3+}	3.334 1	999 999.0
Ba^{2+}	9.117 3	426.1
O^{2-}	−3.257 6	49.8
XX^-	−2.971 07	100.0

inner region (region I) and an outer region (region II). In the inner region the lattice configuration is evaluated explicitly while the outer region can be viewed from the defect as a continuum. The displacements within the outer region are due solely to the electric field produced by the total charge of the defect centered at the defect origin. The Mott-Littleton method[29] is employed in the outer region.

In our calculations the perfect lattice is initially relaxed to equilibrium, and a region of crystal containing several hundred atoms is equilibrated around the specified defect and dopant configuration. The derivation of the potential parameters A, ρ, C, Y, and k for $YBa_2Cu_4O_8$ is described in Ref. 33 and the values of the parameters are given in Table I. Our potentials can reproduce the crystallographic structure of $YBa_2Cu_4O_8$ with the difference from the experimental data being less than 1.3%. The potential parameters for the dopant ions are taken from Ref. 34 and are given in Table II. We note that our potential is an ionic empirical potential with no screening. Hence we do not expect this potential to give good structural changes on doping in cation-doped $YBa_2Cu_4O_8$, as changes due to doping on the metallic planes or chains are due to more than ionic sizes and charges. However, it is possible for this potential to give reasonable structures for the pure-T_c superconductor $YBa_2Cu_4O_8$, and this potential can give quick indications of the doping sites, although the displacements calculated using this potential may not be justified.

TABLE II. Potential parameters for doping ions. $C = 0$ for all interactions.

	Short-range interaction	
	A (eV)	ρ (Å)
Zn^{2+}-O^{2-}	499.6	0.3595
Ce^{4+}-O^{2-}	1013.6	0.3949
Pr^{4+}-O^{2-}	1226.0	0.3871
Th^{4+}-O^{2-}	1147.7	0.3949

	Shell-model parameters	
Species	Y (e)	k (eV Å^{-2})
Zn^{2+}	2.05	10.28
Ce^{4+}	5.85	116.0
Pr^{4+}	6.54	103.61
Th^{4+}	7.28	193.1

RESULTS AND DISCUSSION

In this study we examined the various dopants Zn^{2+}, Ce^{4+}, Pr^{4+}, and Th^{4+} substituting at the Y^{3+}, Ba^{2+}, or Cu^{2+} sites. We ignored the effect of defect interactions leading to possible aggregation; the results presented therefore refer to systems at low dopant concentrations. We also neglected the contribution of vibrational defect entropies to the free energy of the solution. Given these assumptions, the energies of the solution were obtained by combining appropriate cohesive energies with lattice-energy terms accompanying the formation of the substitutional species.

We first consider the dissolution of divalent dopant Zn^{2+} into the Y^{3+}, Ba^{2+}, or Cu^{2+} sublattice. The defect reactions for the dissolution of divalent dopants into the Y^{3+}, Ba^{2+}, or Cu^{2+} sublattice can be represented by the following defect equations (note that in the Korger-Vink notation[35] used in this paper, vacancies, interstitial, and substitutional atoms are denoted as V_{Cu}, Cu_I, and M_{Cu}, respectively):

$$MO + Y_Y^X \rightarrow M_Y' + \tfrac{1}{2}Y_2O_3 + \tfrac{1}{2}V_O^{\cdot\cdot} , \quad (4)$$

$$MO + Ba_{Ba}^X \rightarrow M_{Ba}^X + BaO , \quad (5)$$

$$MO + Cu_{Cu(1)}^X \rightarrow M_{Cu(1)}^X + CuO , \quad (6a)$$

$$MO + Cu_{Cu(2)}^X \rightarrow M_{Cu(2)}^X + CuO , \quad (6b)$$

where M denotes the divalent dopant. For dopant substitution at the Y^{3+} site, oxygen vacancies are created to preserve charge neutrality.

The substitution energies for dopant substitution at Ba, Y, Cu(1), and Cu(2) sites are reported in Table III. The lattice energies and energies of vacancies used in calculation are given in Table IV. The calculated energies of dissolution per dopant ion for cation substitution for different doping sites are given in Table V. (This energy is also called the solution energy. The smaller the solu-

TABLE III. Substitution energies in $YBa_2Cu_4O_8$.

	Substitution energies (eV)			
	Zn	Ce	Pr	Th
Ba	−5.62	−49.47	−48.35	−46.97
Cu(1)	3.68	−32.43	−30.14	−29.05
Cu(2)	3.22	−40.56	−37.71	−36.38
Y	25.23	−24.95	−23.26	−21.95

TABLE IV. Lattice energies and energies of vacancies (eV per formula unit).

Lattice energies		Energies of vacancies	
ZnO	−39.43	Ba	18.62
CeO_2	−102.6	Cu(1)	25.62
PrO_2	−101.2	Cu(2)	29.50
ThO_2	−100.1		
CuO	−42.91		
BaO	−31.31		
Y_2O_3	−135.6		

tion energy, the easier is cation doping.) Our calculations show that Zn^{2+} has the lowest solution energy at the Cu(2) site, indicating that the Zn^{2+} cation energetically prefers to substitute at the Cu(2) site. This result is consistent with experimental results.[21–23]

For tetravalent dopants Th^{4+}, Pr^{4+}, and Ce^{4+} substituting at the Y^{3+}, Ba^{2+}, or Cu^{2+} sites, the charge-compensating mechanism has to be considered. For tetravalent dopants Th^{4+}, Pr^{4+}, and Ce^{4+} substituting at the Ba^{2+} site, there are two possible charge-compensating defects: oxygen interstitial or barium vacancies. The corresponding defect reactions with oxygen-interstitial charge compensation and barium-vacancy charge compensation are represented by Eq. (7a) and Eq. (7b), respectively:

$$MO_2+Ba^X_{Ba}\rightarrow M^{\cdot\cdot}_{Ba}+BaO+O''_I\ , \tag{7a}$$

$$MO_2+Ba^X_{Ba}\rightarrow M^{\cdot\cdot}_{Ba}+2BaO+V''_{Ba}\ , \tag{7b}$$

where M denotes the tetravalent dopant. To determine the most favorable charge-compensating mechanism, we should compare the solution energies of the defect reactions with different charge-compensating mechanisms. For tetravalent dopants Th^{4+}, Pr^{4+}, and Ce^{4+} the defect reaction (7a) was calculated to have a lower solution energy than the defect reaction (7b) (see Table V) and hence the defect reaction (7a) is predicted to be the major compensating mechanism. The probable site of the oxygen interstitial (where the energy is the lowest) was taken to lie along the line joining the two barium sites, taking into account structural and charge-distribution symmetries. The lowest energy of −19.80 eV corresponds to the creation of the oxygen interstitial and is used in all subsequent solution-energy calculations.

Similarly, for tetravalent dopants Th^{4+}, Pr^{4+}, and Ce^{4+} substituting at the Cu^{2+} sites two possible charge-compensating defect reactions were found, and the one involving the creation of oxygen interstitials has the defect reaction as follows:

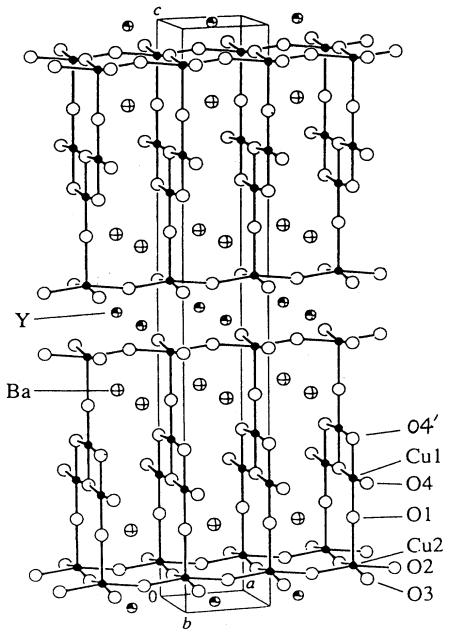

FIG. 1. Structure of $YBa_2Cu_4O_8$.

$$MO_2+Cu^X_{Cu(1)}\rightarrow M^{\cdot\cdot}_{Cu(1)}+CuO+O''_I\ , \tag{8a}$$

$$MO_2+Cu^X_{Cu(2)}\rightarrow M^{\cdot\cdot}_{Cu(2)}+CuO+O''_I\ . \tag{8b}$$

The other involving the creation of copper vacancies has the defect reaction as follows:

$$MO_2+Cu^X_{Cu(1)}\rightarrow M^{\cdot\cdot}_{Cu(1)}+2CuO+V''_{Cu(1)}\ , \tag{9a}$$

$$MO_2+Cu^X_{Cu(2)}\rightarrow M^{\cdot\cdot}_{Cu(2)}+2CuO+V''_{Cu(2)}\ . \tag{9b}$$

It is found that defect reactions (8a) and (8b) are more energetically favorable than the reactions (9a) and (9b), as shown in Table V.

For tetravalent dopants Th^{4+}, Pr^{4+}, and Ce^{4+} substituting at the Y^{3+} site, the defect reaction is given as

$$MO_2+Y^X_Y\rightarrow M^{\cdot}_Y+\tfrac{1}{2}Y_2O_3+\tfrac{1}{2}O''_I\ , \tag{10}$$

with the creation of oxygen interstitials to preserve

TABLE V. Calculated energies of solution (in eV per dopant ion) for cation substitution for Ba, Cu, and Y in $YBa_2Cu_4O_8$. [1] refers to defect reactions for dopant substitution at Ba or copper sites with the creation of oxygen interstitials. [2] refers to defect reactions for dopant substitution at Ba or copper sites with the creation of, respectively, Ba or copper vacancies.

	Solution energies (eV)						
	Zn	Ce		Pr		Th	
		[1]	[2]	[1]	[2]	[1]	[2]
Ba	2.50	2.04	9.16	1.73	8.84	2.04	9.16
Cu(1)	0.20	7.48	9.99	8.34	10.85	8.36	10.87
Cu(2)	−0.26	−0.65	5.74	0.77	7.16	1.03	7.42
Y	6.88	−0.03		0.23		0.47	

TABLE VI. Calculated changes of interatomic distances and interlayer distance (in %) for cation substitution at Y and Cu(2) sites. Negative values indicate shortening and positive values indicate elongation of interatomic distances and interlayer distance.

Dopants doping	site	Cu(1)-O(1)	Cu(2)-O(1)	Cu(2)-O(2)	Cu(2)-O(3)	Cu(1)-O(4)	Cu(1)-O(4′)	Ba-O(1)	Y-O(2)	Y-O(3)	z(Ba)-z[O(1)]
Pr	Y	0.50	−2.04	1.19	1.38	0.29	−0.29	−0.34	−0.84	−1.17	−25.62
Th	Y	0.49	−2.29	1.29	1.49	0.31	−0.30	−0.30	−0.29	−0.63	−26.79
Zn	Cu(2)	−1.37	3.61	1.20	1.73	0.03	−0.45	−0.33	0.12	0.06	37.23
Ce	Cu(2)	−0.71	0.69	6.34	5.87	−0.12	−1.38	2.69	2.27	2.04	−6.13

charge neutrality. Our calculations show that both the Pr^{4+} and Th^{4+} cations have the lowest solution energies at the Y^{3+} site (see Table V), i.e., they prefer to substitute at the Y^{3+} site, which is in agreement with experimental results,[25–27,36] whereas the Ce^{4+} cation has the lowest solution energy at the Cu(2) site, indicating that Ce^{4+} prefers to substitute at the Cu(2) site.

The calculated changes of interatomic distances and interlayer distance for cation doping are given in Table VI (the structure of $YBa_2Cu_4O_8$ is shown in Fig. 1). We observed that Zn, Pr, and Th cause large changes in the interlayer distance of z(Ba)-z[O(1)]. We found that there are structural changes not only in the c direction but also in the a and b directions. For example, there are relative large changes in the Cu(2)-O(2) and Cu(2)-O(3) bond lengths, especially caused by Ce doping. We found that Pr and Th doping cause the opposite changes of the Cu(1)-O(1) and Cu(2)-O(1) bond lengths compared with Zn and Ce doping. Pr and Th doping cause a shortening of the Cu(2)-O(1) bond length and an elongation of the Cu(1)-O(1) bond length, whereas Zn and Ce doping cause an elongation of the Cu(2)-O(1) bond length and a shortening of the Cu(1)-O(1) bond length. It has been reported[33,37–39] that, when $YBa_2Cu_4O_8$ is compressed, the shortening in the Cu(2)-O(1) bond length is much larger than the compression of the unit cell in the same direction [i.e., a shortening of the Cu(2)-O(1) bond length with respect to the compression of the lattice parameter c], and the reduction in the Cu(1)-O(1) bond length is smaller than the compression of the unit cell in the same direction [i.e., a relative elongation of the Cu(1)-O(1) bond length with respect to the compression of the lattice parameter c]. It has been claimed that the enhancement of T_c in $YBa_2Cu_4O_8$ under high pressure is largely due to the changes in the Cu(2)-O(1) bond length with pressure, which may induce charge transfer from the CuO chain to the CuO_2 plane.[37–39] If we think that the charge transfer is also reflected in the changes in the Cu(1)-O(1) and Cu(2)-O(1) bond lengths in cation-doped $Yba_2Cu_4O_8$, then the shortening of the Cu(2)-O(1) bond length and the elongation of the Cu(1)-O(1) bond length caused by Pr and Th doping should result in charge transfer from the CuO to the CuO_2 plane leading to the enhancement of T_c. But Pr and Th doping depress T_c. It appears that not only changes in the Cu(1)-O(1) and Cu(2)-O(1) bond lengths affect T_c but also changes in the other structural parameters in cation-doped $YBa_2Cu_4O_8$.

Table VI shows that in the case of Th doping the Cu(2)-O(2) bond length increases 1.29%, the Cu(2)-O(3) bond length increases 1.49%, and the Cu(1)-O(4) bond length increases 0.31%, indicating the increase of lattice parameters a and b. From the results of changes in Cu(2)-O(1), Cu(1)-O(1), and Cu(1)-O(4′) bond lengths, we also found that Th doping causes Cu(2)-O(4′) bond length to decrease by 0.81%, which results in a decrease in the lattice parameter c. Our results are in qualitative agreement with the experimental finding[25] that Th doping in $YBa_2Cu_4O_8$ causes increase in the lattice parameters a and b and decrease in the lattice parameter c. We found that Ce doping causes even larger changes in lattice parameters a and b. It results in a 6.34% increase of the Cu(2)-O(2) bond length, a 5.87% increase of the Cu(2)-O(3) bond length, and a 0.12% decrease of the Cu(1)-O(4) bond length, indicating that Ce doping causes a larger increase of lattice parameters a and b than Th doping. Similarly, we found that Ce doping causes a 0.39% decrease in the Cu(2)-O(4′) bond length, which also causes a decrease in the lattice parameter c, but this decrease is smaller than that caused by Th doping. Experimental results[24] show that Ce doping in $YBa_2Cu_4O_8$ causes increase in the lattice parameters a and b and decrease in the lattice parameter c. But Ce doping causes larger increase in a and b and smaller decrease in c compared with Th doping. Our results are also in qualitative agreement with these experimental results.

It is known that Zn and Cu have the same valence of 2+ and similar ionic size (the ionic size of Zn and Cu are 0.68 and 0.65 Å, respectively). It is expected that Zn doping at the Cu(2) site will cause only a small sublattice displacement. We do find the small displacement at the Cu(2) site ($\Delta x = \Delta y = 0$ and $\Delta z = 0.0005$ Å). But it is surprising that the displacements of O(1) and Cu(1) are the largest among the dopants under study, with Δz values of 0.0830 and 0.0576 Å, respectively. The large displacements of O(1) and Cu(1) result in a 3.61% increase in the Cu(2)-O(1) bond length and a 1.37% decrease in the Cu(1)-O(1) bond length. Increase in the Cu(2)-O(1) bond length and decrease in the Cu(1)-O(1) bond length are expected to induce reverse charge transfer from the CuO_2 plane to the CuO chain, leading to the depression of T_c. We note that Zn doping causes the largest increase of the Cu(2)-O(1) bond length and largest decrease of the Cu(1)-O(1) bond length among group-1 and -2 dopants. It is not clear if these largest bond-length changes are responsible for the fact that Zn doping has the largest depression rate of T_c (Refs. 22,23) among the dopants under study.

CONCLUSIONS

Using computer-simulation techniques, we studied Zn, Ce, Th, and Pr doping in $YBa_2Cu_4O_8$. We found that the

Zn cation energetically prefers to substitute at the Cu(2) site whereas Pr and Th prefer to substitute at the Y site. These results are in agreement with the experimental results. Our results also suggest that Ce preferentially substitutes at the Cu(2) site. Analysis of the structural changes caused by Zn, Ce, Th, and Pr doping was made. We found that Pr and Th doping cause similar structural changes, but Zn and Ce doping result in different structural changes compared with Pr and Th doping. Our calculated changes in lattice parameters due to Th and Ce doping are in qualitative agreement with the experimental results.

[1]B. Bucher, J. Karpinski, E. Kaldis, and P. Wachter, Physica C **157**, 478 (1989).
[2]E. N. van Engige, R. Griessen, R. J. Wijngaarden, J. Karpinski, E. Kaldis, S. Rusiechi, and E. Jilek, Physica C **168**, 482 (1990).
[3]D. Braithwaite, G. Chouteau, G. Martinez, J. L. Hodeau, M. Marezio, J. Karpinski, E. Kaldis, S. Rusiecki, and E. Jilek, Physica C **178**, 75 (1991).
[4]J. J. Scholtz, E. N. van Eenige, R. J. Wijngaarden, and R. Griessen, Phys. Rev. B **45**, 3077 (1992).
[5]R. G. Buckley, J. L. Tallon, D. M. Pooke, and M. R. Presland, Physica C **165**, 391 (1990).
[6]T. Sakurei, T. Wada, N. Suzuki, S. Koriyama, T. Miyatake, H. Yamanchi, N. Koshizuka, and S. Tanaka, Phys. Rev. B **42**, 8030 (1990).
[7]I. Mangelschots, M. Mali, J. Roos, H. Zimmermann, and D. Brinkmann, Physica C **172**, 57 (1990).
[8]E. T. Heyen, M. Cardona, E. Kaldis, J. Karpinski, S. Rusiecki, and E. Jilek, Physica C **185**, 1749 (1991).
[9]M. Knupfer, N. Nucker, M. Alexander, H. Romberg, P. Adelmann, J. Fink, J. Karpinski, E. Kaldis, S. Rusiecki, and E. Jilek, Physica C **182**, 62 (1991).
[10]S. Pradhan, D. Mcdaniel, A. Kiling, W. Huff, and P. Presland, Physica C **165**, 391 (1990).
[11]D. E. Morris, A. P. Marathe, and A. P. B. Sinha, Physica C **169**, 386 (1990).
[12]I. Felner, I. Navik, U. Yaron, E. R. Bauminger, and D. Hechel, Physica C **185**, 1117 (1991).
[13]Y. Kodama, S. Tanemura, Y. Yamada, and T. Matsumoto, Physica C **199**, 1 (1992).
[14]Y. Kodama, Y. Yamada, N. Murayama, M. Awano, and T. Matsumoto, in *Advances in Superconductivity III*, edited by K. Kajimura and H. Hayakawa (Springer, Tokyo, 1991), p. 399.
[15]T. Wada, T. Sakurai, N. Suzuki, S. Koriyama, H. Yamauchi, and S. Tanaka, Phys. Rev. B **41**, 11 209 (1990).
[16]T. Ishigaki, F. Izumi, T. Wada, N. Suzuki, Y. Yaegashi, H. Asano, H. Yamauchi, and S. Tanaka, Physica C **191**, 441 (1992).
[17]R. S. Liu, J. S. Ho, C. T. Chang, and P. P. Edwards, J. Solid State Chem. **92**, 247 (1991).
[18]X. Zhang and C. R. A. Catlow, Modelling Simulation Mater. Sci. Eng. **1**, 45 (1992).
[19]X. Zhang and C. R. A. Catlow, Phys. Rev. B **47**, 5315 (1992).
[20]X. Zhang, Physica C **222**, 227 (1994).
[21]I. Felner and B. Brosh, Phys. Rev. B **43**, 10 364 (1991).
[22]Takayuki Miyatake, Koji Yamaguchi, Tsutomu Takata, Naoki Koshizuka, and Shoji Tanaka, Phys. Rev. B **44**, 10 139 (1991).
[23]S. P. Pandey, M. S. Hegde, B. V. Kumaraswamy, and A. V. Narlikar, Physica C **206**, 207 (1993).
[24]I. K. Gopalakrishnan, J. V. Yakhmi, and R. M. Iyer, Physica C **204**, 413 (1993).
[25]I. K. Gopalakrishnan and J. V. Yakhmi, Physica C **218**, 457 (1993).
[26]P. Berastegui, L.-G. Johansson, M. Kall, and L. Borjesson, Physics C **204**, 147 (1992).
[27]S. Adachi, N. Watanabe, N. Seiji, N. Koshizuka, and H. Yamauchi, Physica C **207**, 127 (1993).
[28]H. B. Liu, D. E. Morris, A. P.B. Sinha, and G. H. Kwei, Physica C **223**, 51 (1994).
[29]*Computer Simulation of Solids*, edited by C. R. A. Catlow and W. C. Mackrodt, Lecture Notes in Physics Vol. 166 (Springer-Verlag, Berlin, 1982).
[30]J. Chem. Soc. Faraday Trans. 2 **5** (1989).
[31]B. G. Dick and A. W. Overhauser, Phys. Rev. **112**, 90 (1958).
[32]M. J. Norgett and A. B. Lidiard, in *Computational Solid State Physics*, edited by F. Herman, N. W. Dalton, and T. R. Coehler (Plenum, New York, 1972), p. 385.
[33]X. Zhang and C.R. A. Catlow, Physica C **193**, 221 (1992).
[34]G. V. Lewis and C. R. A. Catlow, J. Phys. C **18**, 1149 (1985).
[35]F. A. Kroger and H. J. Vink, Solid State Phys. **3**, 307 (1956).
[36]Zhen Guo, Nobuyoshi Yamada, Ken Ichiro Godaira, Takeo Iri, and Kay Kohn, Physica C **220**, 41 (1994).
[37]E. Kaldis, P. Fischer, A. W. Hewat, E. A. Hewat, J. Karpinski, and S. Rusiecki, Physica C **150**, 668 (1989).
[38]R. J. Nelmes, J. S. Loveday, E. Kaldis, and J. Karpinski, Physica C **172**, 311 (1992).
[39]Y. Yamada, J. D. Jorgensen, Shiyou Pei, P. Lightfoot, Y. Kodama, T. Matsumoto, and F. Izumi, Physica C **173**, 185 (1991).